Article

Damage Propagation and Residual Strength of Simple Block-Loaded CFRP Plates with Circular Holes under Tension–Tension Fatigue Conditions

Lukas Heinzlmeier *[ID]**, Stefan Sieberer** [ID]**, Thomas Wolfsgruber** [ID]**, Christoph Kralovec** [ID] **and Martin Schagerl** [ID]

Institute of Structural Lightweight Design, Johannes Kepler University Linz, Altenberger Straße 69, 4040 Linz, Austria
*   Correspondence: lukas.heinzlmeier@jku.at

Abstract: Holes and their effects on the fatigue behavior and damage propagation of thin-walled structural components remain objects of research. In this paper, the previously untreated effect of round holes in thin plain-woven carbon fiber-reinforced plastic plates subjected to simple block loading is examined, and the implication on both damage propagation and residual tensile strength is investigated. Using three-dimensional digital image correlation, the damage propagation in the performed experimental tests is acquired, and the damage size is quantified. The evaluations reveal a relationship between the damage propagation and applied load level, for which an empirical model has been previously established by the authors. As the number of cycles increases, a saturation behavior is found. Once the increased load is imposed on the plate, damage propagation resumes, leading to further damage propagation that can be described with the same empirical model as the initial damage propagation, including renewed saturation behavior. The subsequent experimental tests to determine the residual tensile strength reveal a positive effect of the existing damage size, as the ultimate load significantly exceeds the ultimate load of the non-damaged plate.

Keywords: CFRP plate; circular hole; fatigue testing; simple block loading; damage propagation; digital image correlation; residual tensile strength

1. Introduction

The requirements for the thin-walled components used in lightweight applications are constantly increasing. In the design of such components, numerous factors (e.g., operational environment, acting loads, and safety) must be considered to achieve the highest performance for the defined weight targets. Independent of the chosen material, variations in thickness, fillets, notches, and cutouts must be addressed during the design phase. There is usually a special interest in circular holes because they are used to join different parts (e.g., with bolts) or let electrical wires and fluid-containing lines pass through [1]. These holes may significantly affect the load-bearing capacity of the structures with their presence as they cause stress concentrations. For thin-walled metallic components, the influence of the holes is already well known [2,3].

In contrast, the consideration of the holes in carbon fiber-reinforced composites is more challenging. Compared to metals, these materials are not isotropic. Instead, they are composed of multiple stacked layers, where each layer is generally orthotropic and can ideally result in quasi-isotropic laminates. The significance of holes in laminates resulted in the definition of a standardized procedure named the open-hole tensile test, which is designated ASTM D 5766/D5766M-95 [4]. This involves the static testing of rectangular coupons and gives the open-hole tensile strength [4].

An early approach to consider the effect of a hole in a laminate utilizing a static stress criterion was made by Whitney and Nuismer [5]. Subsequent investigations modified these approaches so that more accurate approximations could be carried out [6–9]. However, all

these approaches require extensive experimental investigations to identify the required parameters, as they depend on the laminate architecture and hole size. Wallner et al. [10] also propose a modified approach based on Whitney and Nuismer [5]. They reduce the experimental effort using a numerically calculated critical path curve and the maximal stress inside the laminate. A further well-documented means of analyzing the stresses in laminates is the finite element method (FEM). It is frequently chosen as the validation method to verify new proposed approaches [11,12].

Nevertheless, these approaches and the standardized procedure do not cover cyclic loading. The stacked architecture and the different properties of fibers and matrix cause a complicated fatigue damage behavior, involving matrix cracks, debonding between matrix and fibers, delaminations, and fiber breakage [13,14]. Some coupon-level experimental studies investigating these fatigue mechanisms have recently been published [15–17]. Nixon-Pearson et al. [18] investigated fatigue damage progression in CFRP coupons with holes and observed damage in the form of matrix cracks and delaminations originating from the free edge and the hole edge of the coupon. Damage propagation proceeded from both edges into the laminate and then towards the clamping zones until a complete collapse of the coupons was observed. These findings are in agreement with those of Aymerich et al. [19], who also specified that the matrix dominated failure modes cause damage in notched carbon/epoxy laminates. The latter also emphasizes the damage-dependent decrease in the stress concentration at the hole. Very high numbers of cycles were necessary to lead to a failure of the coupons, while for plates with circular holes, Heinzlmeier et al. [20] revealed that the matrix-dominated damage modes were also the primary mechanism of damage growth under tension–tension loading conditions, but due to the large considered specimen size, no complete collapse was reached as damage propagation halted and saturated.

However, as real structures experience multiple load levels, this must be addressed in the design phase to specify the maximum allowable loads and service intervals. According to the research of van Paepegem et al. [21], no general answer regarding the loading, i.e., whether high-low or low-high loading is more damaging to the structure, can be given, as some researchers consider low-high loading to be more critical [22], while others consider high-low loading to be more critical [23]. In their review, Post et al. [24] provided commonly used methods to describe the fatigue of multiple loaded composite materials without holes. More recently, a model describing the multiple load levels and their effects on fatigue behavior and residual strength was developed [25]. However, holes are not considered in this model. Broughton et al. [26] studied the effect of varying the load level on the fatigue life in glass fiber-reinforced plastic specimens with holes, where a relationship between the fatigue life and the surface temperature, longitudinal strains, and stiffness was perceived.

Often, the reduction in stiffness is used to determine the progressive damage [18,26,27]. In practice, measuring stiffness reduction can be difficult, i.e., damage originating from the holes must be assessed differently. One option is to describe the damage propagation in the laminate by measuring the damage size.

This present paper builds on this approach. Based on the work of Heinzlmeier et al. [20], this research paper investigates the propagation in pre-damaged thin plain-woven CFRP plates with a circular hole exposed to simple block loading. All loading designations are consistent with those of Schijve et al. [28]. The focus of this present paper is placed on experimental investigations. Tests were performed under sinusoidal tension–tension loading conditions. Damage size was measured using contact-free measuring techniques, which include three-dimensional digital image correlation (3D-DIC) and active pulse thermography (APT). Furthermore, a previously published empirical model [20] was applied to the simple block-loaded experimental measurements to investigate its applicability. A further objective of this work was to investigate the residual tensile strength and how it is affected by the presence of damage caused by preceding simple block loading.

The innovative contribution of this research contrasts existing publications [18,19,29] in which experimental investigations have been carried out using holed coupons with

small dimensions (which adopted the state-of-the-art approach). This research is focused on wide plates as test specimens, where a large number of load cycles were performed. The use of plates was motivated by the fact that, in real applications, the components of large dimensions are predominantly used instead of narrow, tensile-test-specimen-shaped components. As a result of the large dimensions of the plates, the free edges are located far from the hole, and no interaction between the free edges and the hole exists. This means that the effect of the hole on the fatigue behavior can be analyzed independently.

This paper starts with a methodology section that explains the experimental setup, procedure, and damage assessment. Moreover, the empirical model used to describe damage propagation is presented. In Section 3, the damage propagation of simple block-loaded plates with a circular hole and the validation of the empirical model with the experimentally obtained data are given. Additionally, the results of the damage-size-dependent residual tensile strength are presented. The final part of this paper includes a discussion of the results, followed by our concluding remarks.

2. Materials and Methods

As this study builds on the results and findings by Heinzlmeier et al. [20], the same experimental setup and specimens in the form of plates with a circular hole were used. They are presented in the following.

2.1. Experimental Setup and Procedure

Four prepreg layers of a plain woven CFRP fabric (Solvay, Brussels, Belgium) *CY-COM*®970, 3k-T650, in arrangement $[0f/45f]_s$, fiber volume fraction $\phi = 0.6$) were used, composite blanks with a thickness of 0.816 mm were cured in an autoclave (12 h, 0.9 MPa, 120 °C), and plates with circular holes were cut out by water jet cutting. This manufacturing method has been reported to have negligible influence on the fatigue behavior [30]. Subsequent inspection using ultrasonic flaw detection (UFD) and APT were carried out to check for potential defects during hole machining. The final sanding and adhesive bonding of the clamping tabs completed the specimen preparation. Figure 1 shows a plate with a circular hole (diameter 20 mm), where the prepared region (the white surface with black speckles) for measuring the surface displacements with 3D-DIC and the placement of the clamping tabs are indicated.

The experimental investigations were carried out using a *Zwick-Roell*® (Ulm, Germany) 100 kN servo-hydraulic cylinder and a CUBUS control unit at a load ratio R = 0.1 and a cyclic frequency of 4 Hz. A load cell allows for control and adaption during load-controlled testing. In Table 1, the defined load levels of the tested plates for simple block loading are provided since, for the current investigation, the chosen plates remained in the fixture once 2000k cycles had been reached, and a second loading block with the same R-value and cycle number but different cyclic load amplitude was initiated. The number of cycles for the tensile fatigue tests is typically 1 million cycles [18]. However, for the tests performed in this study, this number increased to 2 million cycles for each loading. We chose this number because this clearly reveals the damage behavior. The theoretical static ultimate tensile load (UTS) of the plate with a circular hole (34.58 kN) is calculated by scaling up the results of the coupon tests (40 mm width, identical length, and lay-up) to the plate width according to the classical laminate theory, utilizing a stress concentration factor of 3 for the hole. The resulting UTS represents the peak load of a plate cycled with 100% and is equivalent to the normalization coefficient used to define the normalized load level *x*.

After completing the simple block loading (4000k cycles) the plates were considered run-outs and were statically tested to determine the residual tensile strength. Therefore, the plates were unloaded down to 500 N and a static ramp with a load rate of 1 kN/s was specified.
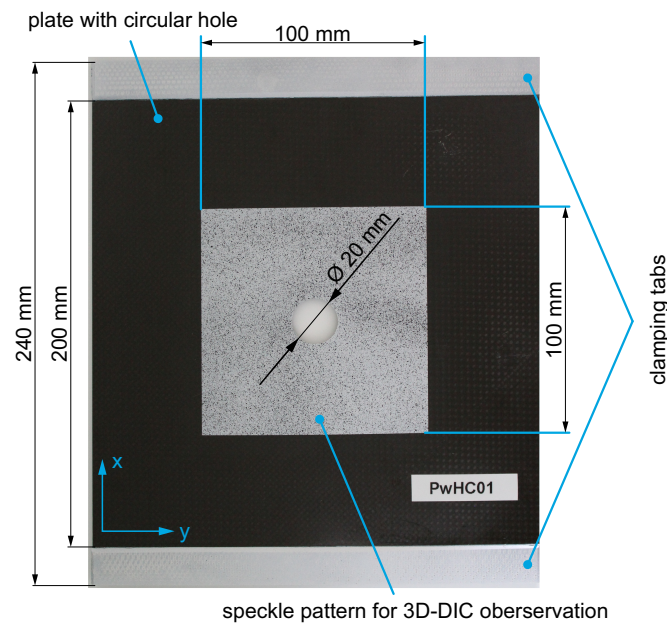
Figure 1. Layout and dimensions of a plate with circular hole with the clamping tabs and speckle pattern applied.

Table 1. Specified load levels for the tested plates; four plates are subjected to simple block loading with stress ratio R = 0.1.

Normalized Load Level x		Mean Load	Amplitude
0.7	*I*	13.31 kN	10.89 kN
0.8	*II*	15.22 kN	12.45 kN
0.9	*III*	17.12 kN	14.01 kN
1.0	*IV*	19.02 kN	15.56 kN

Plate No.	Load level to assess damage propagation	
	20k–2000k	2000k–4000k
1	*I*	-
2	*I*	*III*
3	*II*	-
4	*II*	*IV*
5	*II*	*III*
6	*III*	*IV*
7	*IV*	-
8	*IV*	*II*

As a consequence of the large plate width, an in-house designed fixture was used. This fixture consists of two parts, the lower part is mounted on the test rig, while the upper part is attached to the load cell, which is connected to the loading cylinder. The rotation around the cylinder axis is suppressed by guiding bars. The experimental setup, including specimen, loading, and measuring equipment (3D-DIC and APT) are shown in Figure 2.

A 3D-DIC system from *Correlated Solutions* (Irmo, SC, USA) was used to assess damage propagation. For this purpose, the 3D-DIC system was placed on the test rig and focused on the area surrounding the hole where the speckle pattern was applied. The 3D-DIC system was supplied with the load signal from the CUBUS control unit, which used it as a trigger signal. For the APT measurements a $\mu\varepsilon^{®}$ (Ortenburg, Germany) TIM 450 thermal imager and an *Elinchrom*® (Renens, Switzerland) Zoom Pro flash head were used. The APT thermal imager was positioned facing the 3D-DIC system, focusing on the opposite face of the plate. During the entire test, the position of the measuring equipment remained unchanged.
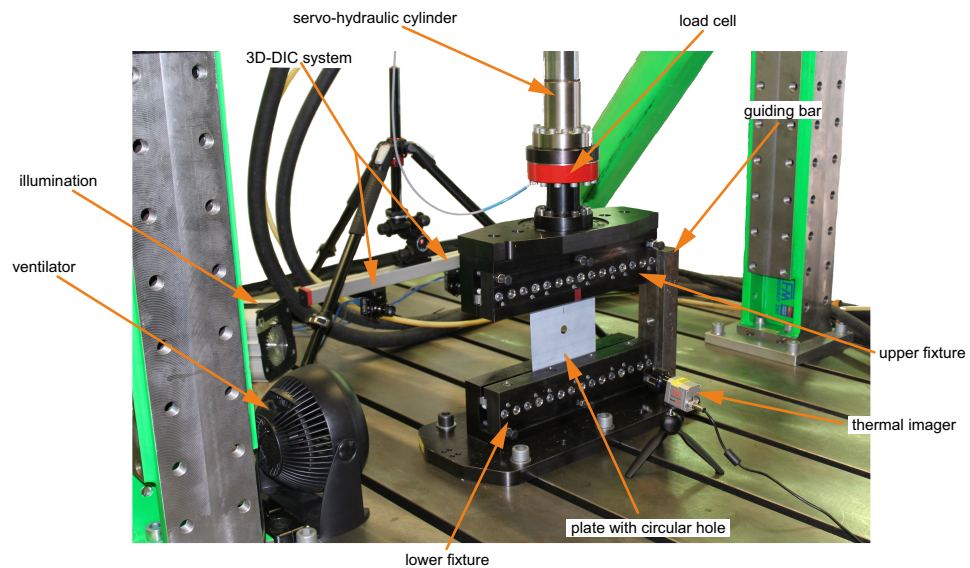
Figure 2. Experimental setup to perform the simple block-loading tests.

In order to acquire data with the 3D-DIC system, images were captured in 500-cycle intervals throughout cyclic testing at peak load. Intermittently, the cyclic loading was paused, and static loading ramps from 500 N to 15 kN at a rate of 1 kN/s were inserted. These static loading ramps were captured separately using the 3D-DIC system. At the end of each static loading ramp, APT measurements were performed.

These APT measurements were started immediately before activating the excitation source and stopped after 5 s. An acquisition frequency of 10 Hz was used to capture damage that became visible as a result of an interrupted heat flow.

2.2. Damage Assessment

To quantify the possible damage, the 3D-DIC output variable *Sigma* (first-standard-deviation confidence interval for the match at the evaluation points, in pixels) was taken anew. For each plate, the first image at peak load, taken from the initial loading, was selected as the reference image. A sequential processing of all 3D-DIC images captured at peak load provided a measurement of the damage propagation for the individual plates by considering the area of the damage (expressed with 3D-DIC *Sigma*). This was carried out by picking the subset size (29 px = 1.556 mm) and step size (7 px = 0.3756 mm) for the evaluation since this selection gives the best compromise between accuracy and noise. Output values exceeding the threshold of the 3D-DIC *Sigma* are classified as being damaged. The sum of all damaged evaluation points with attached (finite) areas gives the area of damage at a certain cycle number. The threshold value of 3D-DIC *Sigma* was chosen by matching the resultant area of damage with measurements from APT and UFD (C-Scan) made on the first tested plate [20]. It was revealed that *Sigma* = 0.1 is a suitable threshold value, which was used again throughout this research.

The evaluation of each static loading ramp with the 3D-DIC system was performed using the same subset size (29 px), step size (7 px), and threshold value. However, each loading ramp was processed separately, whereby the reference image was taken at the beginning of each ramp.

The evaluation of the APT measurements were carried out using MATLAB, where two subsequent images (one before and one after excitation) were subtracted to eliminate the interfering heat and reveal the possible damage.

By comparing the measurements of 3D-DIC and APT taken at the same cycle count and under the same loading conditions, a validation of the selected threshold value of *Sigma* can be performed. This procedure was demonstrated by the authors in a previous publication [20].

2.3. Empirical Model for Damage Propagation

The applied empirical model to describe damage propagation originating from a circular hole in the thin plain-woven CFRP laminates is taken from [20]. There, from the experimental investigations on identical plates, an empirical model was established that can describe damage propagation after damage initiation due to tension–tension loading. Equation (1) gives the number of cycles N as a function of the area of damage A and the three parameters C_0, C_1, and C_2, with which the damage propagation acquired using 3D-DIC were adjusted.

$$N(C_0, C_1, C_2) = \frac{C_0\, A^{C_1}}{C_2 - A} \tag{1}$$

The parameters in Equation (1) were fitted from test data and, thus, are only valid for the given laminate and hole geometry. Because of the use of identical specimens, it is assumed that the same coefficients can be used for all tested loading cases. The subsequent determination of the functional dependency of each parameter with respect to the normalized load level x finally yielded the representation, as shown in Equation (2) [20].

$$N(x) = \frac{50}{x^{18.9}} \frac{A^{3.14\,x}}{0.127\, e^{6.28\,x} - A} \tag{2}$$

The detailed methodology to derive this empirical model and the underlying assumptions were described in more detail in Heinzlmeier et al. [20]. Applying this empirical model and taking the normalized load level x (defined in Section 2.1) together with the area of damage A as a variable, leads to the paths depicted in Figure 3. Therefore, the area of damage A is plotted over the number of cycles (i.e., axes entries are swapped). The representation is bounded to 4000k cycles, since the performed experimental tests are stopped at this number of cycles and the residual tensile strength is determined. The progressive damage shows a clear saturation behavior when the stress level is constant.
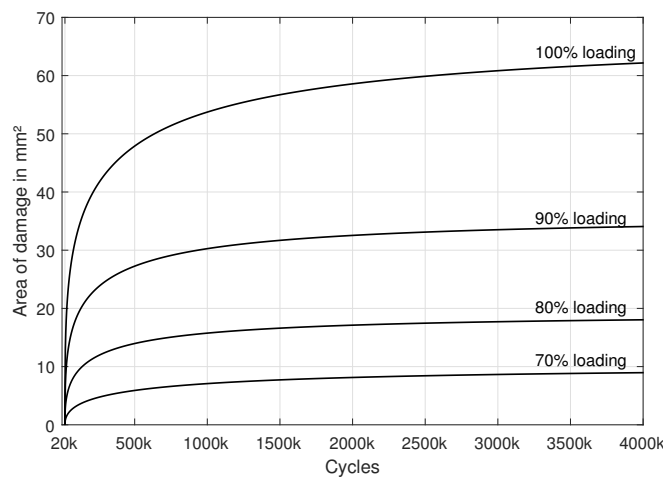

Figure 3. Paths of the empirical damage propagation model for the selected load levels.

3. Results

In this section the results of the simple block-loaded fatigue tests, the validation of the empirical damage propagation model and the results of the static residual tensile strength tests are presented.

3.1. Measured Damage Size Due to Proper Threshold Value Selection

To ensure that the selected threshold value of the 3D-DIC variable *Sigma* has been chosen correctly and that there are no changes in the speckle pattern caused by unknown influences throughout the entire test duration, a validation of the selected threshold value is necessary. This is achieved by matching the 3D-DIC computations with the equivalent

measurements obtained with APT at the same number of cycles and at the identical load (15 kN).

Figure 4 compares the 3D-DIC computations and APT measurements at the last static ramp at the final pause (4000k, 15 kN). The scaling of the 3D-DIC and APT measurements is kept unchanged for all measurements.
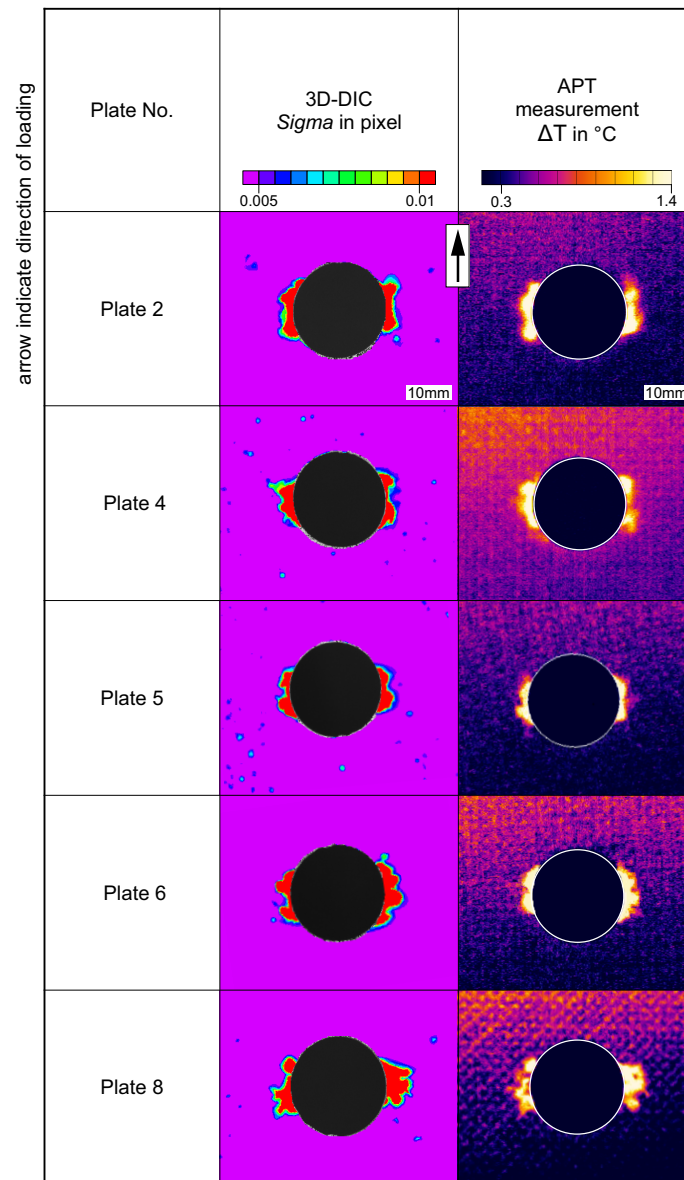

Figure 4. Validation of the selected threshold value of *Sigma* by comparing 3D-DIC computations and APT measurements at the last static ramp (i.e., after 4000k cycles at a static load of 15 kN).

The 3D-DIC computations demonstrate that with *Sigma* = 0.1 the red (damaged) areas are consistent with the APT images even at 4000k cycles and that choice is valid. Varying the threshold value affects the outcome only from the range of 0.005 and 0.15, but there is no longer a match with the APT measurements. Within 0.005 and 0.15, the use of *Sigma* exhibits no effect on the area of the damage expressed with it. This can be attributed to an abrupt transition between the damaged areas and non damaged regions.

3.2. Damage Propagation of Simple Block Loaded Plates with a Circular Hole

The measured 3D-DIC damage propagations during the simple block loading of the plates are illustrated in Figure 5. There, the area of damage is plotted against the

number of cycles. The damage propagation for the first loading block (20k–2000k cycles) is also included. The initial 20k cycles were classified as damage initiation and are not included [20]. These damage propagations were the basis for calibration of the model represented in Equation (2). The second loading block (2000k to 4000k cycles) was used to validate the proposed empirical model for simple block-loading fatigue behavior.
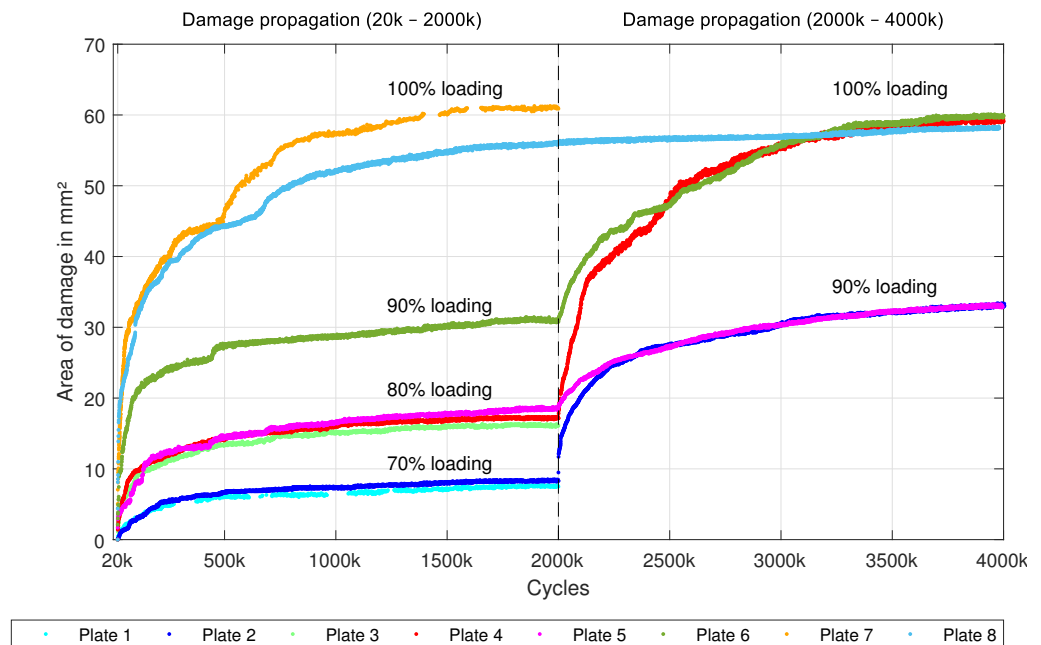

Figure 5. Damage propagation in plates with a circular hole under simple block tension-tension loading conditions evaluated via 3D-DIC.

In the first loading block, all investigated plates show saturation regarding the area of damage. The subsequent increase in the cyclic load amplitude causes an immediate effect on the damage propagation behavior. As shown in Figure 5, damage propagation continues in those plates, which are exposed to higher loads in the simple block-loading tests. Plates 2, 4, 5, and 6 exhibit similar behaviors, where, at the beginning, the damage propagation is affected by jumps, and as the number of cycles increases, the damage area reveals a stagnation in growth. For the plates where the load was increased to 100%, the jump-like propagation is more noticeable and continues over a longer period of testing. Plates 2 and 5, along with Plates 4 and 6, demonstrate that in saturation, the areas of damage are governed by the load level and not the loading history. This is evident in the comparison of Plate 2 and Plate 5 with Plate 6. Plate 2 has been tested for 2000k cycles at a 70% load and 2000k cycles at 90%. Plate 5 was loaded with 80% and with 90%. A comparison of the final area of damage to that of Plate 6 at 2000k cycles (90% load) highlights that a similar area of damage is reached.

Moreover, this can be also observed by comparing Plate 4 (4000k) and Plate 6 (4000k) with Plate 8 (2000k). However, for Plate 8, which has been loaded with a higher load (100%) in the first load block and later cycled at a lower load (80%), no further change to the damage size is found. As a result, the area of damage of Plate 8 remains unchanged after 2000k and 4000k cycles. Regarding the final area of damage, that of Plate 8 appears to be smaller. However, if Plate 7 had been subjected to a load reduction for simple block loading, it seems that the area of damage would match better than those of Plate 4 and Plate 6 (at 4000k).

3.3. Validation of the Empirical Damage Propagation Model

The load increase in the simple block loading causes further damage propagation, which, in turn, is characterized by a fast initial growth, a saturation behavior, and a load-

level-dependent final area of damage. To account for the non-zero initial damage area at the beginning of the simple block loading (2000k), a shift is required to apply the empirical damage propagation model from Section 2.3. Therefore, the evaluated areas of damage at 2000k cycles are taken as starting points and are used to intersect with the empirical model (when the load is adapted). The paths of the empirical model (depicted in Figure 3) are shifted towards these starting points by offsetting them along the number of cycles so that the area of damages coincide (empirical model and 3D-DIC evaluated damage at 2000k). A graphical representation of the empirical damage propagation model and the evaluated damage propagations (3D-DIC) are depicted in Figure 6. Since a certain level of damage exists when adaptation to simple block loading is performed, the paths of the empirical model below these intersecting points are drawn as dot-dashed lines. In addition to this graphical representation, where the paths of the empirical damage propagation model show excellent correlation, Table 2 confirms this by showing the coefficient of determination R^2 of both loading blocks. In addition, the cycles into which the paths are shifted are listed. Here, the negative prefix indicates a backward shift (starting point = 2000k). Since the load on Plate 8 is reduced during simple block loading, this shift approach is not applicable. Consequently, it is not possible to determine a coefficient of determination or a shift cycle number (indicated with *).
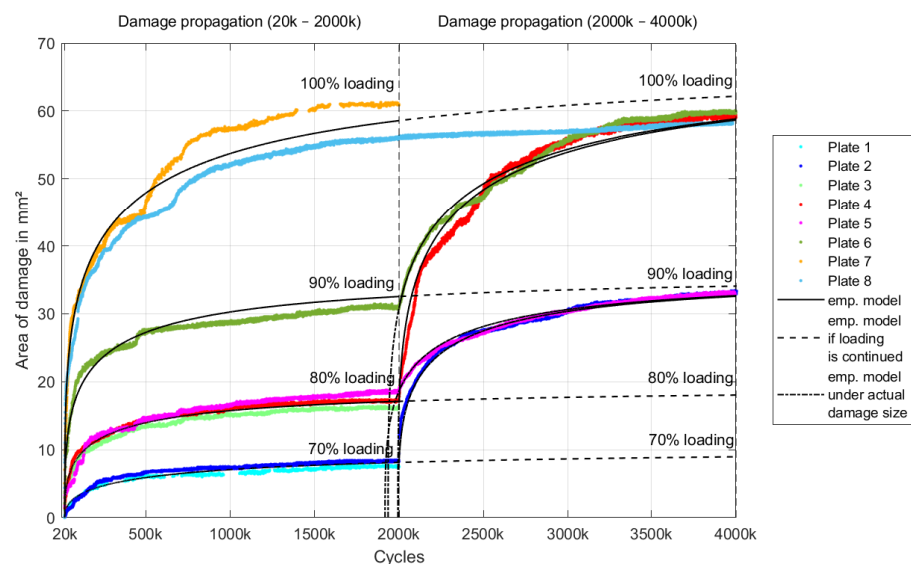

Figure 6. Validation of the empirical damage propagation model with the measured area of damage for simple block-loaded plates with a circular hole.

3.4. Residual Tensile Strength

Subsequent to the cyclic testing, the residual tensile strength is determined via quasi-static loading. In Table 3, the results of the residual tensile strength tests are presented. The numbering of the plates, the applied load levels, the final damage sizes (last measured value at peak load during simple block loading, as shown in Section 2.2), and the associated residual tensile strength values are listed. Furthermore, Figure 7 illustrates the measured residual tensile strengths over the corresponding damage sizes. A static test on a pristine plate proves that the calculated initial strength is appropriate. The resulting experimentally determined static strength (35.07 kN) is also given in Figure 7.

Table 2. Validation of the empirical damage propagation model by using the coefficient of determination R^2.

Plate No.	Coefficient of Determination R^2		Shift in Cycles
	20k–2000k	2000k–4000k	
1	0.944	—	—
2	0.967	0.961	−5263
3	0.924	—	—
4	0.984	0.915	−6951
5	0.921	0.938	−83132
6	0.914	0.909	−64954
7	0.871	—	—
8	0.886	*	*

Table 3. Area of damage at the end of simple block loading and the residual tensile strength from subsequent quasi-static testing.

Plate No.	Load Levels %		Final Area of Damage in mm^2	Residual Tensile Strength in kN
2	70	90	33.11	41.515
5	80	90	32.93	40.627
4	80	100	59.07	45.991
6	90	100	59.85	47.705
8	100	80	56.32	43.622

The residual strength results for the cyclic damaged plates show an increase in the tensile strength compared to that of the pristine plate. It seems that the residual strength increases monotonically with the increase in the final area of damage.
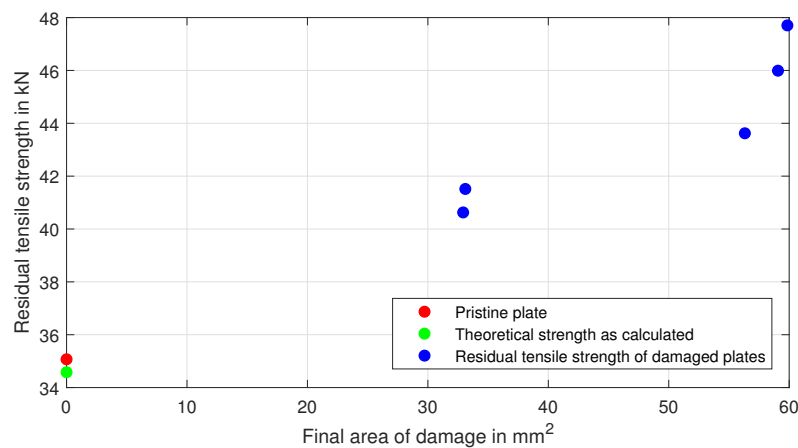

Figure 7. Residual tensile strength after simple block loading (4000k) in plates with a circular hole.

4. Discussion

Discussion of the experimental findings on the propagation of damage in plates with a circular hole and the utilization of the empirical model is given in this section. Moreover, the effect on the residual tensile strength and the possibility to predict damage propagation with the empirical model is discussed.

4.1. Damage Propagation

With the second loading block, damage propagation at two different load levels was assessed. The growth of the damage in the second loading block exhibited a similar behavior as the first loading block. Dependent on the load level, a fast growth at the beginning and a

saturation behavior was observed with increasing the test duration. The measurements performed using active thermography provide additional information, although, in this investigation, thermal imaging was used to validate the 3D-DIC-evaluated area of damage. As a result of the fatigue loading at a low frequency (4 Hz), no noticeable increase in the temperature of the specimens was observed throughout the entire test series. Likewise, the conducted measurements via active thermography, where the temperature increase did not exceed 3 °C, did not cause any thermal stresses; thus, the influence of any thermal stresses on the mechanical response could be excluded.

The underlying damage mechanisms include in-plane interlaminar stresses from differing fiber orientations and the opening of existing delaminations under load conditions. Similar to the first loading block, the second loading block experienced jump-like damage propagation. It is assumed that the frequency of the jumps is governed via stochastic and sudden damage propagation events. Only the damage propagation of Plate 8 was different to that of all other specimens. Here, a lower load was chosen for the second loading block and revealed that the damage remained static. This implies that in the case of HI-LO simple block loading, no further damage propagation takes place.

However, this outcome presumes that the damage size is larger than that which can be achieved at the reduced load level. In these specific situations, only the higher load level is relevant. Physically, this can be explained by the fact that as a result of the cyclic loading with a reduced load, already formed matrix cracks and delaminations do not open entirely, interlaminar shear stresses are reduced, and, thus, no further damage propagation is possible.

In case the damage caused by the higher load level has not yet exceeded that of the lower load level, a reduction in the load could potentially cause further but slower damage propagation. This is only possible if the load level is changed quickly since, after approximately 150k cycles, the damage size of the higher load level exceeds that of the lower load level (saturated damage size).

To address the question regarding which simple block loading is more critical (HI-LO or LO-HI) the results of Plates 2 and 5 can be compared. Here, the loadings were selected inversely (i.e., 80 % and 100 %, and 100 % and 80 %, respectively). Both variants are found to reach the same level of damage, which indicates that neither of the two cases was more critical. However, for reliable conclusions, additional plates must be tested with this procedure of inversely loading the plates.

4.2. Empirical Model for Damage Propagation

Based on the same plates, the empirical damage propagation model presented in Section 2.3 was derived by the authors in a previous study. Thus, this empirical model could be used without need for parameter modification. To account for the existing damage, the paths of the empirical model were shifted. A graphical comparison (see Figure 6) of the paths (empirical model) with the evaluated 3D-DIC damage propagations revealed good correlation. This was also confirmed by the corresponding coefficient of determination R^2. The occurring jumps within the damage propagation are not covered in the empirical model, but since these are seen as random, they could be tolerated.

Besides this procedure, in which the paths of the empirical model were shifted into the last value obtained before load adaptation, a further procedure is feasible. Here, only the paths of the empirical model were considered by shifting the paths into the last calculated value (with the empirical model at 2000k). For Plate 2 and Plate 4, no difference was found since the area of damage determined with 3D-DIC is consistent with that of the empirical model. In contrast, for Plate 5, the coefficient of determination R^2 deteriorated, while for Plate 6, it improved.

Since the load was reduced in Plate 8 and no damage propagation was detected throughout the entire loading block, a shift as described was not possible because there was also an offset within the area of damage (reduced load could not reach the damage size of this higher load). Thus, a shift with respect to the damage size must be performed. An

alternative procedure would be to simply use the damage size after the first loading block and transfer it to the second loading block (which would be a horizontal line in Figure 6).

4.3. Residual Tensile Strength

In the experimental investigations in terms of the residual tensile strength, a relationship with the area of damage was found. As the area of damage becomes larger, the residual tensile strength also increases. It appears that there is a monotonic relationship. This outcome, which is presented in Table 3 and in Figure 7, is in agreement with the findings of Aymerich et al. [19] and Kress and Stinchcomb [31]. Both emphasized a relationship between the number of cycles and the residual tensile strength.

This positive effect of the damage size on the residual tensile strength could be ascribed to a similar phenomenon, as it appears within the fatigue strengthening effect. Relevant investigations on small needled ceramic matrix composite samples revealed a damage-dependent increase in the residual tensile strength [32,33]. Nevertheless, holes were not addressed.

The load-carrying capacity of the plate with a circular hole is primarily provided by the fiber bundles aligned along the direction of loading. In the residual tensile strength tests, the occurrence of fiber breakage triggers immediate total failure. Any static or cyclic loading below that will mostly activate matrix-dominated failure modes, which have, in the case of delamination damage, been observed to propagate into saturating damage growth. Amongst the mechanisms potentially contributing to this effect, two are mentioned. On the one hand, a reduction in the stress concentration factor by changing the geometry of the hole may occur. On the other hand, a local increase in the tensile strength occurs due to fiber bundle alignment in the loading direction (enabled via the matrix failure-driven isolation of fiber bundles from the surrounding laminate). Although this may give a higher stress concentration factor, the benefit of the isolated fibers is more significant in this case. Both mechanisms were detected via the 3D-DIC system and led to an increased residual tensile strength compared to that of the pristine plate.

Considering the increase in the residual tensile strength, it might be possible to raise the cyclic loading to more than 100% (=theoretical UTS of a pristine plate). To address this possibility, further experimental tests are required, where the load is raised once a certain damage size is present. Likewise, to examine a relationship with the fatigue strengthening effect, more experimental testing is required.

4.4. Prediction of Damage Propagation

As a result of the good agreement between the empirical damage propagation model and the evaluated damage propagation paths, it is assumed that the empirical model has a wider applicability. Alternating block (loading blocks are repetitive) and multi-block loading (more than two load levels) should be possible to apply the empirical model. One adjustment is the starting damage size in the empirical model for each new loading block, which must be adapted to match the existing damage size measured from the experimental tests (as performed in this present study), or the final damage size predicted by the empirical model in the previous loading block. Additional experimental investigations must be performed to demonstrate the validity of the empirical model and prove that the empirical model can be applied.

5. Concluding Remarks

This study discussed the damage propagation and residual tensile strength of thin plain-woven CFRP plates in the $[0f/45f]_s$ configuration, with a circular hole subjected to simple block tension–tension loading. Experimental tests were carried out to assess damage propagation using contact-free measuring systems (3D-DIC and APT) to investigate the effect of a load modification on the damage propagation. The damage propagation, which reached saturation at a single load level, was reactivated from a load increase and showed a highly comparable damage propagation behavior to that of the same single load level.

Load reduction, in contrast, has no effect on damage propagation. The application of an empirical damage propagation model, adapted to the first loading block only, demonstrated the usability of the model even in simple block-loading tests. This empirical model gives the number of cycles as a function of the area of damage and may be used to predict the damage propagation under block-loading conditions.

Additionally, the residual tensile strength was examined. It was found that with increasing damage size, the residual tensile strength of the plate was raised. Consequently, the load-carrying capacity of the plate was increased, and it appears as if cyclic loading beyond the initial ultimate tensile load is possible (when a certain damage size is present). To obtain more general knowledge on damage propagation under multi-block-loading conditions and on a functional relationship of the damage size on the residual tensile strength, further experimental research is necessary. For this purpose, other laminates (different laminate thickness and lay-up orientations), hole diameters, plate dimensions, and loadings (compression and shear) have to be taken into account. Further experimental investigations have to be undertaken to determine the statistical reliability of the proposed empirical damage propagation model. For this purpose, the length of the load blocks should be varied to determine this influence on the fatigue behavior of plates with a circular hole.

References

1. Niu, M.C.-Y. *Airframe Structural Design: Practical Design Information and Data on Aircraft Structures*; Conmilit Press: Hong Kong, China, 2011; ISBN 9789627128090.
2. Jafari, M.; Ardalani, E. Stress concentration in finite metallic plates with regular holes. *Int. J. Mech. Sci.* **2016**, *106*, 220–230. [CrossRef]
3. Folias, E.S.; Wang, J.J. On the three-dimensional stress field around a circular hole in a plate of arbitrary thickness. *Comput. Mech.* **1990**, *6*, 379–391. [CrossRef]
4. *ASTM D 5766/D 5766M-95*; Standard Test Method for Open Hole Tensile Strength of Polymer Matrix Composite Laminates. ASTM: West Conshohocken, PA, USA, 2003.
5. Whitney, J.M.; Nuismer, R.J. Stress Fracture Criteria for Laminated Composites Containing Stress Concentrations. *J. Compos. Mater.* **1974**, *8*, 253–265. [CrossRef]
6. Karlak, R.F. Hole effects in a related series of symmetrical laminates. In *Proceedings of Failure Modes in Composites III*; American Society of Metals: Chicago, IL, USA, 1977; pp. 105–117.
7. Kim, J.-K.; Kim, D.-S.; Takeda, N. Notched Strength and Fracture Criterion in Fabric Composite Plates Containing a Circular Hole. *J. Compos. Mater.* **1995**, *29*, 982–998. [CrossRef]
8. Kim, S.-Y.; Koo, J.-M.; Kim, D.; Seok, C.-S. Prediction of the static fracture strength of hole notched plain weave CFRP composites. *Compos. Sci. Technol.* **2011**, *71*, 1671–1676. [CrossRef]
9. Hwan, C.-L.; Tsai, K.-H.; Chen, W.-L.; Chiu, C.-H.; Wu, C.M. Strength prediction of braided composite plates with a center hole. *J. Compos. Mater.* **2011**, *45*, 1991–2002. [CrossRef]
10. Wallner, C.; Almeida, S.F.M.; Kassapoglou, C. Novel criteria for strength predictions of open-hole composite laminates for preliminary design. *Compos. Struct.* **2019**, *229*, 111409. [CrossRef]
11. Wu, H.-C.; Mu, B. On stress concentrations for isotropic/orthotropic plates and cylinders with a circular hole. *Compos. Part B Eng.* **2003**, *34*, 127–134. [CrossRef]

12. Arteiro, A.; Catalanotti, G.; Xavier, J.; Camanho, P.P. Notched response of non-crimp fabric thin-ply laminates: Analysis methods. *Compos. Sci. Technol.* **2013**, *88*, 165–171. [CrossRef]
13. Vassilopoulos, A.P.; Keller, T. *Fatigue of Fiber-Reinforced Composites*; Springer Ltd.: London, UK, 2013; ISBN 9781447126942.
14. Jollivet, T.; Peyrac, C.; Lefebvre, F. Damage of composite materials. *Procedia Eng.* **2013**, *66*, 746–758. [CrossRef]
15. Hallett, S.R.; Green, B.G.; Jiang, W.G.; Wisnom, M.R. An experimental and numerical investigation into the damage mechanisms in notched composites. *Compos. Part A Appl. Sci. Manuf.* **2009**, *40*, 613–624. [CrossRef]
16. Wang, J.; Callus, P.J.; Bannister, M.K. Experimental and numerical investigation of the tension and compression strength of un-notched and notched quasi-isotropic laminates. *Compos. Struct.* **2004**, *64*, 297–306. [CrossRef]
17. Green, B.G.; Wisnom, M.R.; Hallett, S.R. An experimental investigation into the tensile strength scaling of notched composites. *Compos. Part A Appl. Sci. Manuf.* **2007**, *38*, 867–878. [CrossRef]
18. Nixon-Pearson, O.J.; Hallett, S.R.; Withers, P.J.; Rouse, J. Damage development in open-hole composite specimens in fatigue. Part 1: Experimental investigation. *Compos. Struct.* **2013**, *106*, 882–889. [CrossRef]
19. Aymerich, F.; Found, M.S. Response of notched carbon/PEEK and carbon/epoxy laminates subjected to tension fatigue loading. *Fatigue Fract. Eng. Mater. Struct.* **2001**, *23*, 675–683 . [CrossRef]
20. Heinzlmeier, L.; Sieberer, S.; Kralovec, C.; Schagerl, S. Fatigue and progressive damage of thin woven CFRP plates weakened by circular holes. *Exp. Mech.* **2023**, *63*, 871–883. [CrossRef]
21. van Paepegem, W.; Degrieck, J. Effects of Load Sequence and Block Loading on the Fatigue Response of Fiber-Reinforced Composites. *Mech. Adv. Mater. Struct.* **2002**, *9*, 19–35. [CrossRef]
22. Bartley-Cho, J.; Lim, S.G.; Hahn, H.T.; Shyprykevich, P. Damage accumulation in quasi-isotropic graphite/epoxy laminates under constant-amplitude fatigue and block loading. *Compos. Sci. Technol.* **1998**, *58*, 1535–1547. [CrossRef]
23. Gamstedt, E.K.; Sjögren, B.A. An experimental investigation of the sequence effect in block amplitude loading of cross-ply composite laminates. *Int. J. Fatigue* **2002**, *24*, 437–446. [CrossRef]
24. Post, N.L.; Case, S.W.; Lesko, J.J. Modeling the variable amplitude fatigue of composite materials: A review and evaluation of the state of the art for spectrum loading. *Int. J. Fatigue* **2008**, *30*, 2064–2086. [CrossRef]
25. Califano, A.; Dell'Aversano, R. Theoretical approach to the study of fatigue of composites under spectrum loading. *AIP Conf. Proc.* **2018**, *1981*, 020143. [CrossRef]
26. Broughton, W.R.; Gower, M.R.L.; Lodeiro, M.J.; Pilkington, G.D.; Shaw, R.M. An experimental assessment of open-hole tension–tension fatigue behaviour of a GFRP laminate. *Compos. Part A Appl. Sci. Manuf.* **2011**, *42*, 1310–1320. [CrossRef]
27. Muc, A.; Barski, M.; Chwal, M.; Romanowicz, P.; Stawiarski, A. Fatigue damage growth monitoring for composite structures with holes. *Compos. Struct.* **2018**, *189*, 117–126. [CrossRef]
28. Schijve, J. Fatigue damage in aircraft structures, not wanted, but tolerated? *Int. J. Fatigue* **2009**, *31*, 998–1011. [CrossRef]
29. Panella, F.W.; Pirinu, A. Fatigue and damage analysis on aeronautical CFRP elements under tension and bending loads: Two cases of study. *Int. J. Fatigue* **2021**, *152*, 106403. [CrossRef]
30. Montesano, J.; Bougherara, H.; Fawaz, Z. Influence of drilling and abrasive water jet induced damage on the performance of carbon fabric/epoxy plates with holes. *Compos. Struct.* **2017**, *163*, 257–266. [CrossRef]
31. Kress, G.; Stinchcomb, W.W. Fatigue Response of Notched Graphite/Epoxy Laminates. 1985. Available online: https://www.astm.org/stp32788s.html (accessed on 3 September 2023). [CrossRef]
32. Fang, G.; Gao, X.; Yu, G.; Zhang, S.; Chen, J.; Song, Y. Effect of the stress level on the fatigue strengthening behavior of 2D needled C/SiC CMCs at room temperature. *Mater. Des.* **2016**, *89*, 432–438. [CrossRef]
33. Fang, G.; Gao, X.; Zhang, S.; Xue, J.; Song, Y. A residual strength model for the fatigue strengthening behavior of 2D needled CMCs. *Int. J. Fatigue* **2015**, *80*, 298–305. [CrossRef]